Polymer 209 (2020) 122991

Contents lists available at ScienceDirect

Polymer

journal homepage: http://www.elsevier.com/locate/polymer

Characterization of interdiffusion mechanisms during co-bonding of unsaturated polyester resin to thermoplastics with different thermodynamic affinities

Jamal Seyyed Monfared Zanjani *, Ismet Baran **, Remko Akkerman

Faculty of Engineering Technology, University of Twente, 7500 AE, Enschede, the Netherlands

ARTICLE INFO

Keywords:
Thermoset/thermoplastic interphases
Hybrid polymeric composites
Co-bonding

ABSTRACT

Co-bonding of thermoplastics to thermosets remains as a challenge in hybrid composites manufacturing. The interphase of the joint is controlled by the thermodynamic affinity and the processing condition. Thus, the main objective of this study is to describe the interphase formation mechanisms between a thermoset resin and thermoplastics. Therefore, a methodology is developed to predict, control, and analyse the interphase morphology experimentally while modelling approaches are used to assess the microstructure. Hansen solubility parameters are used to select thermoplastics with different thermodynamic affinities to the unsaturated polyester resin as the thermoset. The resin uptake experiments are conducted to identify the kinetics of diffusion and empirical models are recognised to predict the swelling at various processing temperatures. Next, a coarse grain lattice model is established which couples the resin uptake and microscopic observation to extract information on the microstructure of interphase through predicting volume fraction of resin at the interphase.

1. Introduction

Advanced polymeric composites with high strength-to-weight ratio and superior physical properties are proven to be a key component in many technological advancements including aerospace, automotive, energy, and offshore industries. However, polymeric composites have a limited window of properties and major improvements in material and structural designs are necessary for their adaptation to the more demanding applications [1]. One of the practical and promising approaches to extend the applicability of polymeric composites and improve their processability is to use them in the form of the multi-material composites (MMCs). The laminated MMCs are a class of composites in which laminas are made from two or more different material systems. MMCs provides engineers with a design versatility to exploit the best characteristics of each lamina type to the benefit of the specific application. MMCs are the key to meet the ever-growing expectations and requirements for the next generation of structural materials [2].

Various combinations of laminated MMCs have been developed in recent years. Fibre-metal laminates as an alternating arrangement of metallic and fibre reinforced polymeric laminas are well-known in aerospace industry due to their higher impact and fatigue properties and fire resistance [3,4]. Thermoplastic (TP)-Thermoset (TS) hybrid composites are an emerging group of laminated MMCs with significant potentials to address many shortcomings of the current materials. Thermoplastic composites by themselves have received significant attention because of their superior fracture toughness, lower moisture absorption, improved recyclability, weldability, mass production capability and specific performance characteristics over thermoset counterparts [5]. However, the high viscosity of the TP melts and technical limitations to process them into large-scale parts and complex shapes restrict their widespread applications. Alternatively, the lower resin viscosity and well-established technologies for processing TS composites in desired shapes and sizes with well-understood and adjustable properties make them industrially desirable material systems for many applications [6]. Consequently, the combination of these two groups of materials and the development of TP-TS multi-material laminated composites offers a substantial potential for a new generation of advanced composites for demanding applications.

However, the joining of TP to TS is a challenging task with very limited success in achieving effective and industrially relevant welding or joining techniques. The most common joining methods for composites

* Corresponding author.
** Corresponding author.
E-mail addresses: j.seyyedmonfaredzanjani@utwente.nl (J.S. Monfared Zanjani), i.baran@utwente.nl (I. Baran).

https://doi.org/10.1016/j.polymer.2020.122991
Received 25 May 2020; Received in revised form 10 August 2020; Accepted 25 August 2020
Available online 28 August 2020

are mechanical fastening [7], adhesive bonding [8] and welding [9]. However, the applicability of these methods is restricted by the addition of extra weighty metallic bolts and fasteners, damaging the parts during the drilling or polishing steps, thermal degradation under welding condition, necessity for extensive surface preparation, and being labour extensive processes. Direct co-bonding is an alternative promising joining method in which a pre-fabricated part is bonded with TS during the curing process [10]. It is generally accepted that joints formed during the co-bonding and co-curing are strong because they are formed at molecular levels through mechanisms such as entanglements between polymer chains and network formation [10,11].

The quality and morphology of the interphase formed between the pre-fabricated part and the newly cured section play a critical role in the load transfer across dissimilar materials and therefore the overall integrity of the structure. There have been several attempts to provide a better understanding of interphase formation by the interdiffusion during the co-bonding process and possibilities to control it for various TS-TP systems. Rajagopalan et al. [12] studied the diffusion of multi-component epoxy resin into amorphous polysulfone (PSU) applying experimental techniques and they identified diffusion, reaction and phase separation as the phenomena contributing to the size and quality of interphase. They developed a diffusivity model based on free volume theory in polymers to predict and explain the diffusion behaviour and to identify parameters influencing the interphase size [13,14]. Velthem et al. [15] correlated the interphase morphology formed by interdiffusion between RTM6 epoxy resin and poly(ether sulfone) (PES) and phenoxy to the toughness of the overall composite structure. In the phenoxy-RTM6 system due to the broad morphology gradient at interphase, they achieved a toughness improvement of about 100% while the steep interphase morphology in the PES-RTM6 system led to a decrease in toughness value. Voleppe et al. [16] studied the poly(ether sulfone)-RTM6 resin system and they concluded that the depth of the TS diffusion into the TP increased by decreasing the gelation time due to higher thermal activation of diffusion over the curing reaction. Sonnenfeld et al. [17] used engineering semi-crystalline poly-ether-ether-ketone (PEEK) and polyphenylene sulfide (PPS) as a protective coating for epoxy TS matrix. They employed an amorphous thermoplastic sheet of polyetherimide (PEI) as a coupling layer with a high affinity to the epoxy to provide better interaction between layers which increased the adhesion energy by the factor of 15. It is worth noting that in joining incompatible TPs such as PPS and PEEK with TS resins, the joining mechanism is dominated by mechanical interlocking at the surface and load transfer takes place at the interface and not at the interphase [18].

From aforementioned literature, it is currently known that the thermodynamic affinity between TP and TS has a strong effect on the interphase thickness and morphology. Alternatively, processing conditions are identified to be key to control the interphase thickness and morphology between TPs and reactive thermoset resins during the co-bonding process. Besides, interdiffusion of resin molecules into TPs is known to alter the microstructure of TPs by dissolution and swelling leading to a change in the physical and mechanical properties of TPs which influences the diffusion and interphase formation [19]. Nevertheless, the complete understanding of the interdiffusion of a reactive resin into TPs during co-bonding process remains largely uncovered due to the several challenges and complexities concerning: i) the continues change in the molecular weight and molecular structure of the TS resin during the curing process, ii) high dependency of curing reaction and interdiffusion on the environmental condition and iii) unclear diffusion mechanism and post-diffusion phenomena *e.g.* gelation and phase separation.

In this study, interdiffusion of unsaturated polyester resin (UPR) into various TPs is investigated from materials and processing points of view. The research methodology followed here consists of the development of a materials selection principle based on Hansen solubility parameters (HSP) to find suitable TPs with different thermodynamic affinity to the UPR. Material type and processing effects on the interphase morphology and thicknesses are studied using microscopic observations for four selected TPs of polycarbonate (PC), polyurethane (PU), polyvinyl chloride (PVC) and polyetherimide (PEI). The findings are subsequently linked to the cure kinetics, constituent material intrinsic behaviour and TS-TP interactions identified by HSPs. The interdiffusion mechanisms and kinetics are described and connected to the chemo-rheological properties of UPR. The effect of processing temperature, ranging from 4 °C to 60 °C, on the interphase is scrutinized. Models are developed and applied to uncover the process-material-microstructure correlation at TP-TS interphases.

2. Material selection by Hansen Solubility Parameters

TS-TP co-bonding and the interphase qualities are strongly linked to the extent of the interdiffusion between reactive resin molecules and TP chains. The interdiffusion process occurs by the partial dissolution of TP into the resin and diffusion of resin into TP followed by consequent curing of the resin [20,21]. Therefore, thermodynamic compatibility between TS and TP plays an important role in the interphase morphology and size. Herein, a well-known solvent section method named Hansen Solubility Parameters (HSPs) was adapted to select the most compatible TP materials with the UPR and to correlate the TS-TP affinity to interphase size.

HSP employs tabulated interactions of molecules in the form of polar (δ_p), dispersive (δ_d), and hydrogen bonding (δ_h) components to estimate the affinity of material pairs and their solubility [22]. These parameters can be considered as coordinates in a three-dimensional (3D) space, known as the Hansen space. R_0 is defined as the radius of the interaction sphere in Hansen space for a given material which can be calculated empirically for each solute and it is available for numerous industrial polymers in Ref. [22]. Hence, any solvent which lies within the solubility sphere of a solute is expected to dissolve the solute [23].

Furthermore, R_a is defined as the distance in Hansen space between the solvent and solute as [22]:

$$R_a^2 = 4\left(\delta_d^s - \delta_d^p\right)^2 + \left(\delta_p^s - \delta_p^p\right)^2 + \left(\delta_h^s - \delta_h^p\right)^2 \quad (1)$$

where superscripts s and p indicate the solvent and solute, respectively. It is worth noting that the dispersion term is given more weight in Eq. (1) as it is twice important than polar and hydrogen bonding terms in solubility [22,24]. Consequently, a term named relative energy difference (RED) is defined as:

$$RED = R_a / R_0 \quad (2)$$

which is an indication of the interaction between solvent and solute. Here, RED less than one indicates a high affinity between material pairs and their good solubility while RED higher than unity is associated with less favourable interactions. Five TPs namely polymethylmethacrylate (PMMA), PEI, PC, PVC, and PU were considered for co-bonding based on their affinity to UPR and their industrial applicability. Table 1 lists the Hansen solubility parameters for these TPs and also UPR including the calculated Ra and RED values from Eq. (1) and Eq. (2) and their relative affinity levels in connection to UPR [25]. Besides, a 2-D graph approximating the 3D Hansen space is shown in Fig. 1. An approximation was done by combining the polar (δ_p) and dispersive (δ_d) components into a new parameter defined as:

$$\delta_v = \left(\delta_d^2 + \delta_p^2\right)^{1/2} \quad (3)$$

TPs in Table 1 are ordered based on their RED value with respect to UPR. PEI with RED of 1.94 indicated a low affinity to the UPR. The low affinity between PEI and UPR was also perceived in Fig. 1 where UPR was placed outside of the solubility circle of PEI. PU and PVC with RED values slightly higher than unity were showed to have a moderate affinity with the UPR. Likewise, it was confirmed by spotting the UPR at

Table 1
Hansen Solubility Parameters of TPs and UPR, including interaction Radius (R_0), Ra Calculated by Eq .(1) and RED value obtained from Eq (2). HSPs values for TPs are extracted from Ref. [22], and for UPR from Ref. [25].

	δ_d [MPa$^{1/2}$]	δ_p[MPa$^{1/2}$]	δ_h[MPa$^{1/2}$]	R_0[MPa$^{1/2}$]	R_a[MPa$^{1/2}$]	RED	Affinity
UPR	19	17.4	4.2	–	–	–	–
PEI	17.4	4.6	9	7.2	14.2	1.94	Low
PU	17.5	9.6	9.9	8.0	10.11	1.26	Moderate
PVC	16.3	7.8	3.4	7.8	11.3	1.37	Moderate
PC	21.5	9.5	5.1	12.9	9.39	0.73	High
PMMA	19.3	16.7	4.7	17.4	1.04	0.06	Very high

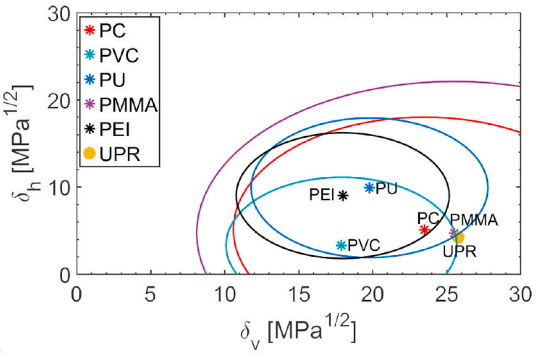

Fig. 1. Two-dimensional (δ_v vs δ_h) diagram showing the extent of TP affinities to UPR.

the borders of PU and PVC solubility circles and towards out of the circles in Fig. 1. Moreover, PC with RED values slightly lower than one and placement of UPR inside their solubility circles conveyed a high affinity to the resin. Besides, PMMA with a very small RED value of 0.06 and a very close location to UPR in HSP alongside its high radius of solubility demonstrated high solubility into the resin. Such a high solubility of PMMA into the resin led to the easy dissolution of PMMA in the resin and therefore PMMA is eliminated from further investigations on interphase formation.

3. Experimental and methods

3.1. Materials

A medium reactive orthophthalic unsaturated polyester resin (UPR) as used [26] which is a resin suitable for resin transfer and vacuum injection moulding processes was used as the thermoset resin. A liquid peroxide based initiator specific for curing of the UPR at room temperature and with long working time (gel time) was utilized as the curing agent. Four TPs of Polyvinyl chloride (PVC) grade CAW with high impact-resistant, thermoplastic elastomer polyurethane (PU) with a shore-A hardness of 80–95 and high abrasion resistance, polycarbonate (PC) high-performance LEXAN™ grade with very high impact resistance and finally polyetherimide (PEI) with commercial name of Ultem as a high-strength amorphous thermoplastic with excellent heat and flame resistance and erosion properties were selected as thermoplastics to be co-bonded with thermosetting UPR.

3.2. Sample preparation and interphase formation

To analyse and quantify the co-bonded interphases, TP specimens were embedded into the UPR. In this regard, cut TPs with dimensions of 15 mm × 15 mm were prepared and their edges were sanded with #500 SiC foil to remove debris followed by washing with a mixture of water, and isopropyl alcohol to eliminate any contamination and residual particles. Specimens were dried in an oven at a temperature of 60 °C for 24 h. The prepared TP specimens were placed upright by using a couple of metallic clamping rings in the middle of a cylindrical embedding mould. Next, the degassed UPR resin mixture was poured onto the TPs until resin completely covered the specimens. To study the effect of temperature on the interphase quality and thickness, co-bonding of selected TPs were conducted at temperatures of 4 °C, 25 °C, 35 °C, 40 °C, 50 °C, and 60 °C. Fig. 2 is a schematic view of the cross-section for the co-bonded specimens and the interphase for TP-TS systems.

3.3. Characterization

3.3.1. Microscopic analysis

The cross-section of interphases were analysed by using a Keyence VHX-5000 digital microscope equipped with a VH-100UR lens. For this, the surface of embedded specimens were polished by using Struers polishing system (Teramin-30) with SiC foil of #500, #1000, #2000 and #4000, in the given order followed by a final polishing by using OP-S NonDry.

3.3.2. Chemo-rheology of resin

The viscosity, storage modulus ($G^{'}$) and loss modulus (G'') of UPR were probed by using the Anton Paar-Physica MCR 501 rheometer in "plate–plate" oscillatory mode with plates of 25 mm diameter and plate-plate spacing of 0.3 mm. All the measurements were conducted applying a strain of 0.5%, and a frequency of 1 Hz. The gel times of the resin at various temperatures as an index of resin cure kinetics were approximated as the crossing point of storage modulus (G') and loss modulus (G'') of UPR mixture with initiator [27]. The gel-time measurements were conducted at different isothermal temperatures of 25 °C, 35 °C, 40 °C, 50 °C, 60 °C, 80 °C and 100 °C. Prior to each measurement and placement of the resin, the rheometer was kept at the set temperature for 30 min to stabilised temperature over the measurement chamber. The temperature dependency of unreactive UPR viscosity (without initiator) was measured between room temperature to 85 °C applying a ramp of 1.5 °C/min.

3.3.3. Surface swelling of TPs by UPR

The swelling of TPs in contact with resin is considered to be a parameter contributing to the interphase formation during the co-bonding TPs and UPR. The swelling of TPs by UPR resin was examined by confining UPR resin between the surface of the TPs sheets and the rheometer head in parallel plate mode as shown in Fig. 3a. This prevented resin flow out due to the capillary forces between UPR and plates. The resin kept for 60 min on the surface of each TP with a set

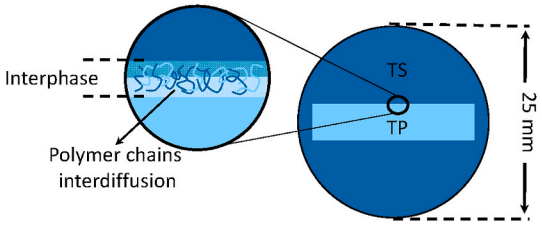

Fig. 2. Schematic view of the co-bonding process with details of the interface region.

plate-plate distance of 0.5 mm. Afterward, the alterations on the surface of TPs were examined by using the Keyence VK-9700 confocal microscope. The confocal microscope had a laser with a wavelength of 408 nm providing spatial and height resolutions of 120 and 1 nm, respectively. Measurements were done on an 8 mm path covering both in-contact to resin and untouched surfaces as shown in Fig. 3b.

3.3.4. Resin uptake and diffusion kinetics

Diffusion kinetics including time and temperature dependencies of resin uptake by each TP were monitored by immersing the TPs into a UPR bath and measuring the changes in their weight. To do so, TPs were cut into estimated sizes of 30 mm × 30 mm. The length, width, and thickness of all the samples were measured using a micrometre with a precision of ±0.01 mm. The weight of the dried samples was measured using an analytical balance with a precision of 0.1 mg. Then, specimens were submerged into the resin by using small metallic clamps. After taking out the specimens from the resin bath, they were washed thoroughly by an excess amount of ethanol and gently cleaned with an absorbent and non-sticking fabric. Then, washed and cleaned samples were left for 10 min at the room temperature to ensure the evaporation of ethanol. The uptake weight, corresponding time and temperature were recorded. The mass uptake per unit area of the contact surface (M*) values were calculated as:

$$M^* = \frac{W_i - W_d}{A} \tag{4}$$

where A was the surface area of TP, W_d was the weight of dry TP specimen, and W_i was the weight after resin uptake. The resin uptake from edges of TP samples was neglected as the lengths and widths of specimens were significantly higher than their thicknesses. To determine the type of transport and its kinetics the resin uptake data were fitted to the Eq. (5) where t was immersion duration, k was an empirical rate constant and n was the transport exponent of diffusion. In Eq. (5), n indicates the type of diffusion in which n = 0.5 represents a Fickian diffusion, $0.5 < n < 1$ is associated with anomalous diffusion, and n = 1 indicates Case II diffusion [28]. The difference in the concentration profile of Fickian and Case II diffusion are shown schematically in Fig. 4.

$$M^* = kt^n \tag{5}$$

Herein, different n and k values were obtained by fitting resin uptake data for each TP at various temperatures. To obtain a model to predict the resin uptake at the different temperatures, temperature-dependent predictive models for k and n in Eq. (5) were considered as Eq. (6). and Eq. (7), respectively.

$$k = k_1 + k_2 T \tag{6}$$

$$n = A_n exp\left(\frac{N_0}{T}\right) \tag{7}$$

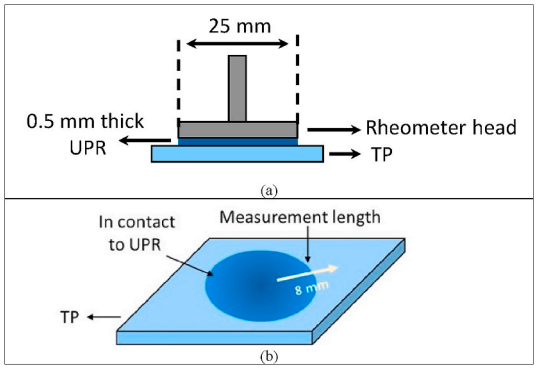

Fig. 3. (a) Schematic presentation of swelling experiment and (b) confocal microscopy measurement path.

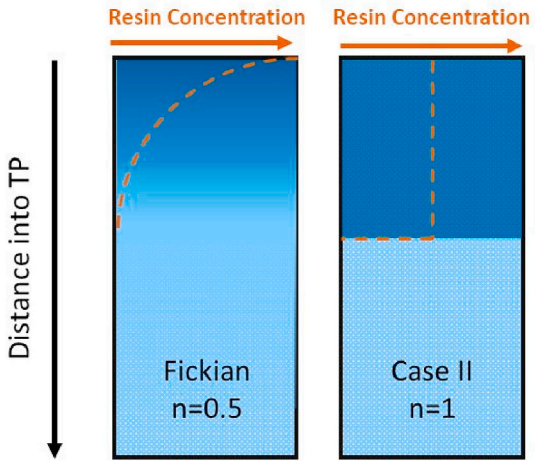

Fig. 4. Schematic representation of (a) Fickian, and (b) Case II diffusion profiles based on n value. (The dashed red lines correspond to the diffusant resin concentration distribution). (For interpretation of the references to colour in this figure legend, the reader is referred to the Web version of this article.)

where T was the temperature, and k_1, k_2, and N_0 were model constants to be acquired through experimental data fitting.

3.3.5. Volume fraction of resin at interphase

The volume fraction of resin at interphase defined as the volume of the diffused resin to the volume of the TP at the interphase region. The volume fraction of resin at interphase is a determining microstructure factor with a huge influence on the mechanical performance of the interphase. However, the volume fraction of resin at the interphase is not easy to measure directly due to the small size of the interphase and complications of high-spatial measurements. Therefore, a prediction method was developed in this section, which used the microscopic measurements of interphase thickness, alongside with diffusion and cure kinetics to determine resin volume fraction at the interphase. In this method, a coarse grain lattice model (CGL) was proposed to imitate the microstructure of interphase in terms of volume fraction of UPR. In CGL, the interphase was divided into distinguished lattice units. It was assumed that each lattice site was occupied by the only one type of material (TP or TS) as it is presented schematically in Fig. 5. In Fig. 5 dark blue lattices represent lattice points filled with UPR and brighter lattice points correspond to TP occupied lattices. The Fig. 5 schematic representation of interphase can be connected to the microscopic views of the interphases as shown in Fig. 6. Herein, the ratio of lattices with dark blue colour to all the lattices presented at the interphase is associated with the volume fraction of resin at interphase. In other words, each lattice raw represents a specific volume fraction of the resin which may differ from a row to another row. To get a single volume fraction value in the CGL model the volume fractions can be averaged over the rows resulting in a single lattice row corresponding to the average volume fraction of the resin over the whole interphase as shown in the bottom of Fig. 5. Doing so, the volume fractions of resin at the interphase became proportional to the length of the resin in the projected array, named as reduced resin volume (V_{UPR}*) to the length of the interface. Thus, to obtain the V_{UPR}* initially Eq. (5), Eq. (6), and Eq. (7) were combined into Eq. (8). Where a model capable of predicting the weight of diffused resin per unit area (M*) for TP of choice at the given time and temperatures within the experimental range was obtained. The constants of Eq. (8) including k_1, k_2, and N_0 were obtained from resin uptake experiments in the previous section.

$$M^* = (k_1 + k_2 T)t^{\left(A_n \exp\left(\frac{N_0}{T}\right)\right)} \tag{8}$$

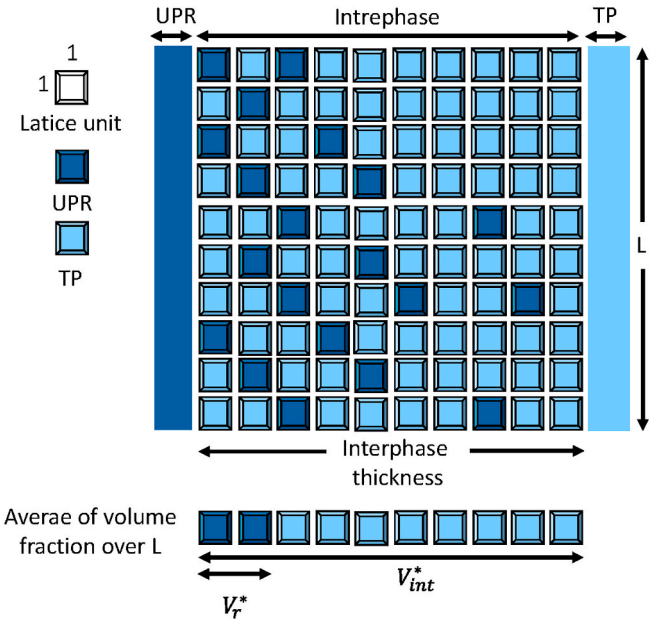

Fig. 5. Coarse grain lattice model for TP-TS interphase microstructure.

Next, a correlation between the reduced volume of the diffused resin (V^*_{UPR}) and M* was established as:

$$M^* = \frac{\rho V_{UPR}}{A} = \rho V^*_{UPR} \tag{9}$$

where A was the surface area of TP in contact to resin, ρ was the density of resin (1.05 gr/cm^3), and V_{UPR} was the volume of diffused resin. Consequently, substituting and rearranging Eq. (8) and Eq. (9) yielded to Eq. (10) which provided the reduced volume of resin at given time and temperature at interphase:

$$V^*_{UPR} = \left(\frac{1}{\rho}\right)(K_1 + K_2 T)t^{\left(A_n \exp\left(\frac{N_0}{T}\right)\right)} \tag{10}$$

The diffusion time in Eq. (10) was estimated by the assumption of termination of diffusion at the gel point of the resin obtained from the chemo-rheology of the resin at different temperatures. On the other hand, interphase thickness obtained through microscopic observations, in the CGL called as reduced interphase volume (V_{int}*) were used to estimate the volume fraction of resin at the interphase (ϕ) as:

$$\phi = \frac{V^*_{UPR}}{V^*_{int}} \tag{11}$$

4. Results and discussion

4.1. Effect of TP type on the interphase size and morphology

Fig. 6 shows the interphase of four TPs, namely PC, PVC, PU, and PEI co-bonded with UPR at 25 °C obtained under the optical microscope. Fig. 6a depicts limited/no detectable interphase for PEI-UPR due to the low affinity of PEI to UPR as predicted by HSPs. On the other hand, PVC formed thin interphase with an average thickness of 35 ± 4 μm because of its moderate affinity to UPR as is seen in Fig. 6b. Alternatively, it is observed in Fig. 6c that PU with similar moderate interaction level as of PVC formed a thicker interphase of 240 ± 11 μm. This difference in the interphase size between PU-UPR and PVC-UPR, while having a similar affinity based on HSPs, may stem from the difference in their physical state at processing temperature. PU was at its rubbery state (glass transition temperature Tg = −25 °C) and PVC was at its glassy state (Tg = 75 °C) at the manufacturing temperature of 25 °C. To elaborate, PU chains at their rubbery state had higher molecular mobility and flexibility which facilitated the penetration and diffusion of the UPR molecules into its structure, whereas the glassy chains of PVC at processing temperature had restricted mobility and therefore reduced diffusivity of the resin. Nonetheless, PC with high affinity to UPR as predicted by the RED of below unity created thick interphase of 430 ± 18 μm as depicted

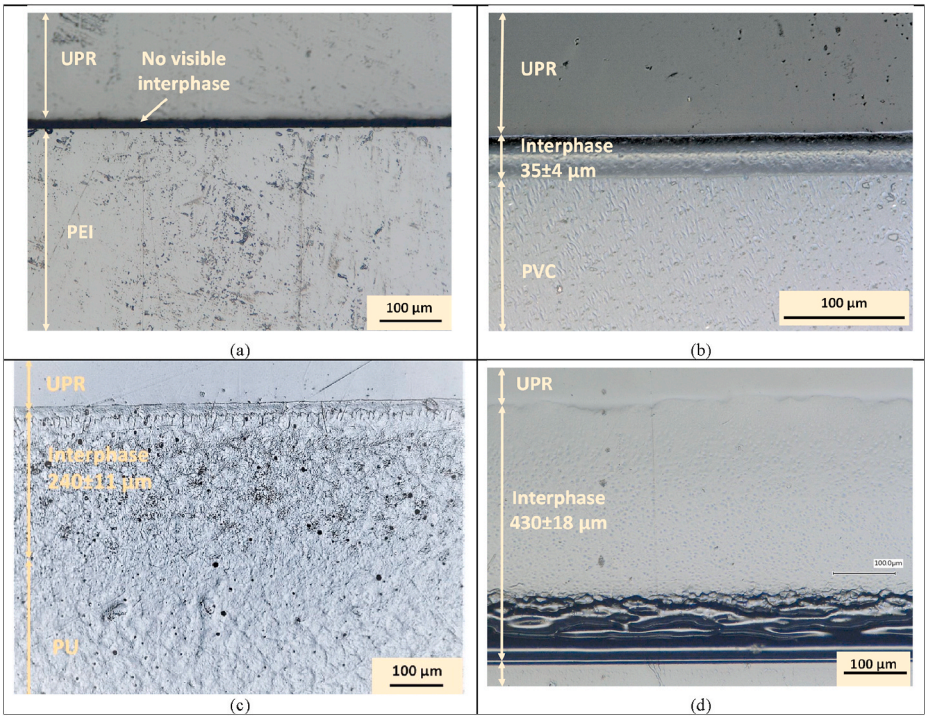

Fig. 6. Microscopic analysis of interphase formation between TPs and UPR at 25 °C for (a) PEI-UPR, (c) PVC-UPR, (d) PU-UPR, (e) PC-UPR.

in Fig. 6d. The morphology of PC-PUR interphase consisted of a dark diffusion front and phase-separated regions representative by a sea-island morphology with small pit-liked indications. The unique sea-island morphology for PC-UPR interphase was detectible with spherical holes as the result of the dissolution of PC chains into resin and consequent phase-separation due to polymerization of the resin. Herein, the small size of islands (pits) implied that phase separation due to the change in the solubility during the resin curing took place after the gelation of resin where the presence of cross-linking bonds kept the domains small [29,30]. The microscopic observation of TP-TS interphases as seen in Fig. 6 demonstrated the close relation between the interphase thickness and morphology by the thermodynamic affinities of material pairs and material physical state. It is worth noting that due to the very low affinity of PEI to UPR and its inability to form interphase with UPR this TP was excluded hereafter from further investigations.

4.2. Effect of processing temperature on the interphase

Fig. 7 reveals the microscopic views of the interphase between selected TPs with UPR at temperatures of 4 °C, 35 °C, 40 °C, 50 °C 60 °C. The interphase morphology of the same TPs at 25 °C are already provided in Fig. 6. Besides, interphase thickness variations by temperature for each TP are projected in Fig. 8.

It was noticed from Figs. 6 and 7 that the PC-UPR interphases at different temperatures displayed similar sea-island morphology but with different interphase thicknesses. Additionally, it was seen in Fig. 8a that the PC-UPR interphase formed at 4 °C had a thickness of 636 ± 15 μm while an increase in temperature to 25 °C sharply reduced the interphase thickness to 430 ± 18 μm. Accordingly, the minimum thickness of 389 ± 5 was obtained at 35 °C. Nevertheless, a further increase in the manufacturing temperature from 35 °C led to a gradual increase in the PC-UPR interphase thickness up to 531 ± 12 μm at 60 °C. These initial reduction and subsequent increase in the interphase thickness for PC-UPR was explained by the changes in the viscosity and gel time of UPR by temperature. The gel time (as an index of curing kinetics and diffusion termination time) and viscosity (as an index of molecular mobility of resin) were measured for UPR at different processing temperatures as presented in Table 2. It is seen that an increase in temperature shortens the gel-time and concurrently reduces the viscosity. However, the degree of these changes were not proportional to

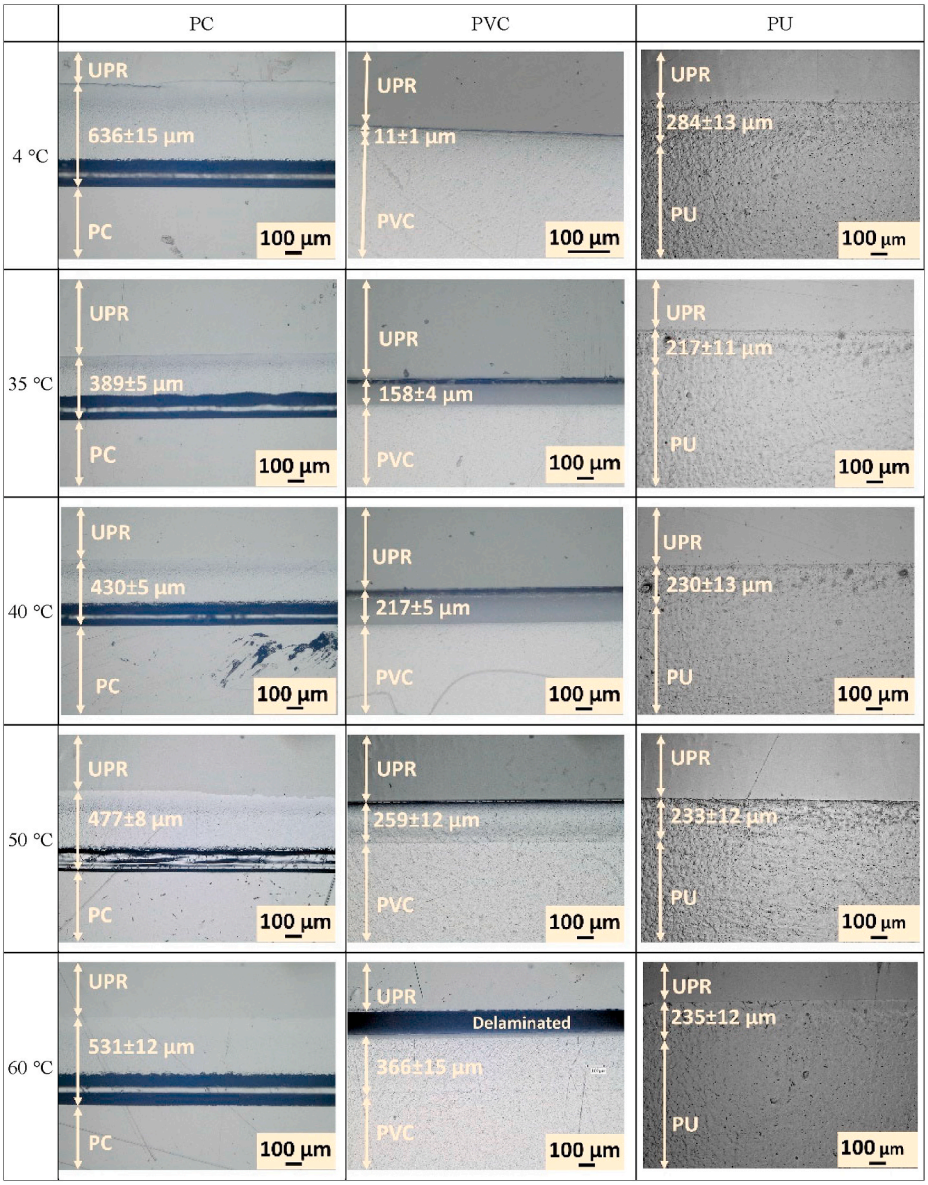

Fig. 7. Microscopic analysis of interphase between TPs and UPR at different temperatures.

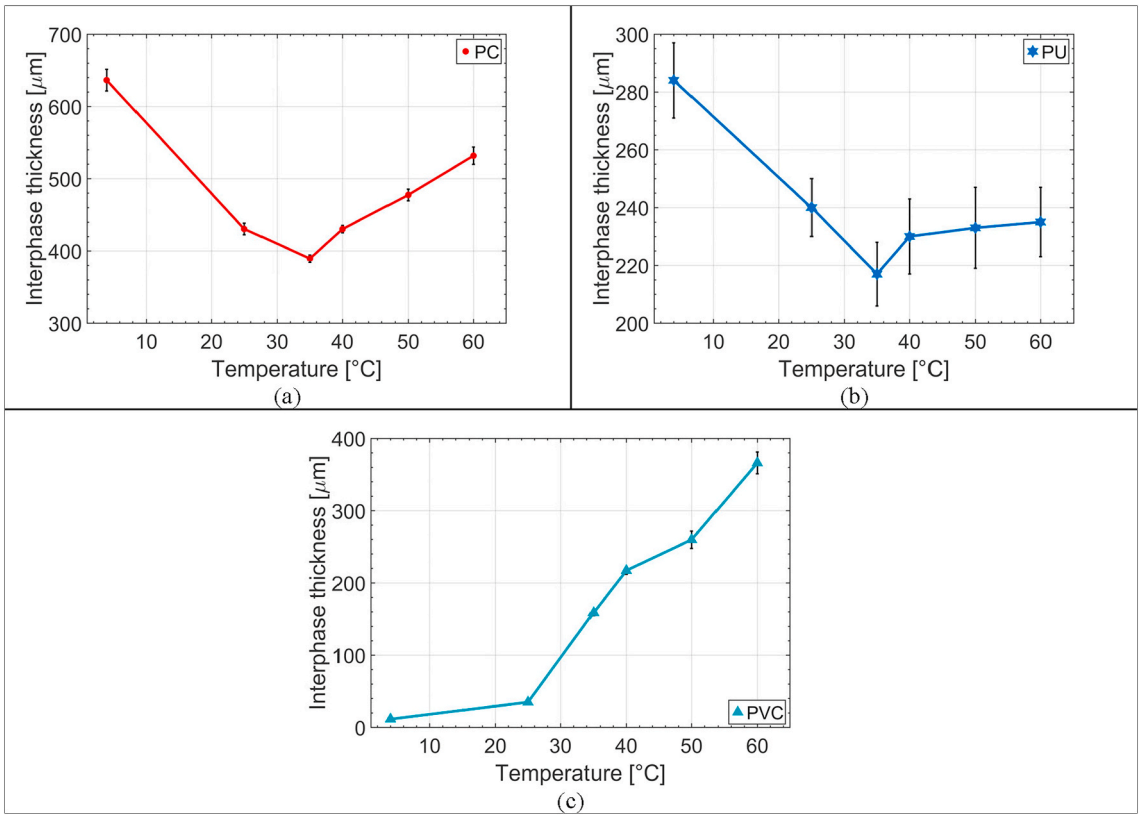

Fig. 8. Effect of temperature on interphase thickness for co-bonded (a) PC-UPR, (b) PVC-UPR, and (c) PU-UPR.

temperature change at different temperatures. To elaborate, an increase in temperature for example from 25 °C to 35 °C at the lower end of temperature range resulted in 8640 s reduction in gel time which significantly limits the diffusion time, while a change from 50 °C to 60 °C only reduced the gel time by 360 s. Therefore, the very thick interphase observed for PC-UPR at 4 °C compared to other temperatures was associated with the expected long cure time for UPR at this temperature which a provided diffusion process with extended time. Hence, the decrease in the interphase thickness from between 4 °C and 35 °C was correlated with a steep decrease in the gel time of the resin in this temperature range. On the other hand, the increase in interphase thickness after 35 °C was associated with a lower level of decrease in gel time while extreme reduction of viscosity of resin as seen in Table 2 which promoted the molecular mobilities and therefore accelerated the diffusion process. Similar temperature dependency trend on interphase thickness was also observed for PU-UPR system where the maximum thickness was observable at 4 °C as 284 ± 13 μm with a sharp decrease to a minimum at 35 °C as 217 ± 5 μm followed by a gradual increase up to 235 ± 12 μm in sample processed at 60 °C as it is shown in Fig. 8b. Contrary, PVC-PUR exhibited an increasing trend on interphase thickness from 4 °C to 60 °C as it is presented in Fig. 8c. The minimum interphase thickness was observed at 4 °C as 11 ± 1 μm and the maximum was at 60 °C reaching a thickness of 505 ± 51 μm. It was also observed that the bonding quality of PVC and UPR degraded by increasing the temperature despite the increase in diffusion thickness with clear delamination signs at higher temperatures as seen in Fig. 7.

Table 2
Rheological characteristics of UPR including gel time and viscosity at different temperature.

	25 °C	35 °C	40 °C	50 °C	60 °C
Gel time [sec]	12,600	3960	1740	840	480
Viscosity [Pa.S]	1.51	0.78	0.58	0.35	0.19

The delamination was occurred because of higher shrinkage of the resin cured at a higher temperature and weak bonding and limited load transfer between PVC-UPR. Nevertheless, the different trend of PVC-UPR interphase thicknesses compared to PC-UPR and PU-UPR was associated to the different mechanisms of diffusion in PVC compared to others which is further elaborated in the following sections by realising the differences in the kinetics of diffusion between TP materials.

4.3. Swelling and surface topology changes

Fig. 9 reveals the surface profile and swelling level of specimens surface examined by confocal microscopy. It was observed that the swelling of TPs is correlated with the affinity of TP and resin. PC with the highest affinity level to UPR showed the highest swelling level as seen in

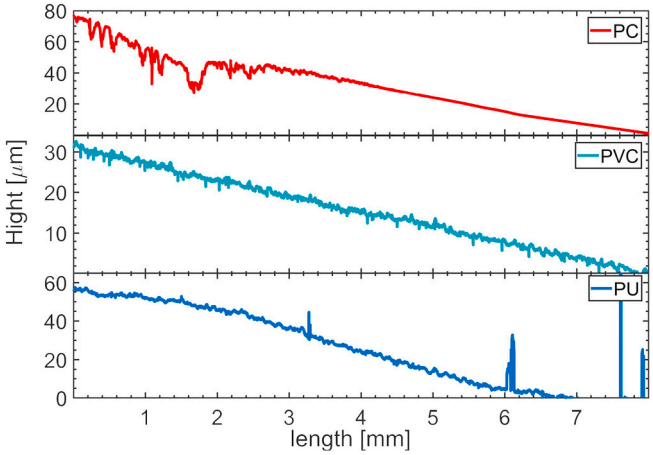

Fig. 9. Surface topology change for TPs after rheometry measurements.

Fig. 9 to be about 80 μm. Alternatively, PU swelled less than 60 μm due to its moderate affinity while being at its rubbery state. PVC with a moderate affinity and at its glassy state swelled about 30 μm. As it is shown in Fig. 3b, surface roughness measurements were performed by taking the middle of the swelling area as the starting point. Therefore, in all the measurements the maximum swelling was observed at the beginning and it decayed toward the end of measurements as it gets closer to boundaries where no resin is presented and lower swelling occurred. Furthermore, Fig. 9 unravelled that there was no significant alteration in the surface roughness for PVC, and PU whereas PC showed an increase in the surface roughness by the formation of abnormalities. The increase in the surface roughness of PC was associated with the dissolution of PC chains into the UPR because of their high affinity. Fig. 10 exhibits the optical images obtained during confocal microscopy of TS which further confirms the extreme surface morphology changes in PC and intact surface roughness for PU and PVC. The solubility of PC in UPR observed here was in agreement with the sea-island morphology formation in the microscopic observation of PC-UPR interphases.

4.4. Kinetics of interdiffusion

Fig. 11a compares the resin uptake (M*) as a function of time for TPs at 25 °C. It is seen that PVC uptake values were significantly lower than the other two TPs of PU and PC. This difference was explained by the moderate affinity of PVC to UPR and being at its the glassy state at 25 °C. On the other hand, PU with a similar moderate affinity to UPR absorbed significantly higher resin which was comparable to PC uptake values. The higher resin uptake by PU compared to PVC was associated with the difference in Tg of PVC and PU which was discussed previously in Section 4.1. PC showed the highest M* values due to its high affinity to UPR. These results were in agreement with the interphase thicknesses measured previously and depicted in Fig. 6 and swelling observations in Fig. 9.

Herein, the empirical model as described in Eq. (5) was applied to assess the rate constant k, and transport exponent n for each TP at different temperatures by line fitting to Ln (M*) vs. Ln(t) data as shown in Fig. 11b–d. Table 3 summaries the obtained n and k values for each TP and at different processing temperatures. It is seen from Table 3 that, n values at 25 °C for PC and PU were very close to 0.5 which indicated the Fickian nature of diffusion while n value for PVC was 0.79 associated with an anomalous diffusion mechanism as depicted in Fig. 4. The different diffusion mechanism in PVC was the contributing factor to its different interphase thickness trend by temperature compared to PC and PU as seen in Fig. 8. To elaborate, in the Fickian diffusion, the driving force for diffusion was the concentration gradient and as it is illustrated in Fig. 4 a concentration gradient was expected at the interphase. Such gradient interphase was noticeable in Figs. 6 and 7 for PU-UPR and PC-UPR [28]. Alternatively, the anomalous diffusion of UPR into PVC resulted in clear diffusion fronts where the concentration of the penetrant drops sharply at the diffusion front as observed in Figs. 6b and 7 [31].

The effect of temperature on diffusion kinetics was examined by conducting resin uptake at temperatures ranging from 25 °C to 60 °C. The obtained results are presented in Fig. 11c and d for PU and PVC, respectively. The calculated n and k values are presented in Table 3. However, it should be noted that due to the high affinity of PC to UPR and its high solubility into the resin no reliable data (negative uptake values) were obtained for PC at elevated temperatures. Therefore PC-UPR diffusion kinetics at a higher temperature than 25 °C was not considered. Nevertheless, it was observed from Table 3 that n value followed a decreasing and k value had an increasing trend with an increase in temperature for both PU and PVC. However, the level of changes in k and n with temperature were significantly different in PU and PVC. The n value for PU decreased from 0.4921 at 25 °C to 0.4461 at 60 °C which corresponds to 0.046 change while it varied remarkably higher for PVC from 0.7901 to 0.5305 equivalent to 0.2595 change. Similarly, k value for PVC increased significantly by an increase in temperature (three orders of magnitude from 25 °C to 60 °C) while PU showed only one order of magnitude change in the same temperature change range. This high dependency of diffusion rate constant and transport exponent to temperature in PVC cleared the observed different trend for PVC-UPR thickness by temperature in Fig. 8.

4.5. Interphase microstructure

Fig. 12 displays the linear trend obtained for n and k based on Eq. (6) and Eq. (7) as a function of process temperature of co-bonding. Table 4 summarizes their calculated constant values based on line fitting on Eq. (6) and Eq. (7). The substitution of these constants into Eq. (10) enabled calculation of the V_{UPR}* for the given material and at the given temperature. Consequently, the volume fraction of resin at the interphase (ϕ) was determined using Eq. (11). Fig. 13 exhibits the ϕ vales for PU and PVC processed at different temperatures. It was found that PVC-UPR interphases had lower resin volume fraction compared to PU-UPR interphases which were in agreement with the aforementioned discussions considering similar affinity of these TPs to UPR while being at different physical states regarding their T_g. Additionally, it is seen in Fig. 13 that the volume fraction of resin at the interphase linearly decreased by increasing the process temperature for both PVC and PU which provide a toolset to predict interphase microstructure cured at different conditions.

5. Conclusions

Within this study, a comprehensive understanding of the effect of materials properties and processing conditions on the interdiffusion and interphase formation of various TPs with UPR during the co-bonding process was obtained. Hansen solubility parameters (HSPs) as a robust

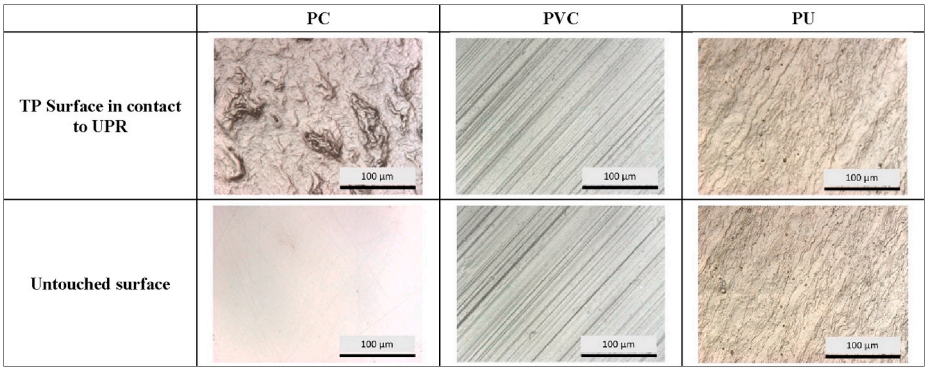

Fig. 10. Microscopic observation after rheometry test on the TP surfaces in contact with resin and untouched surfaces.

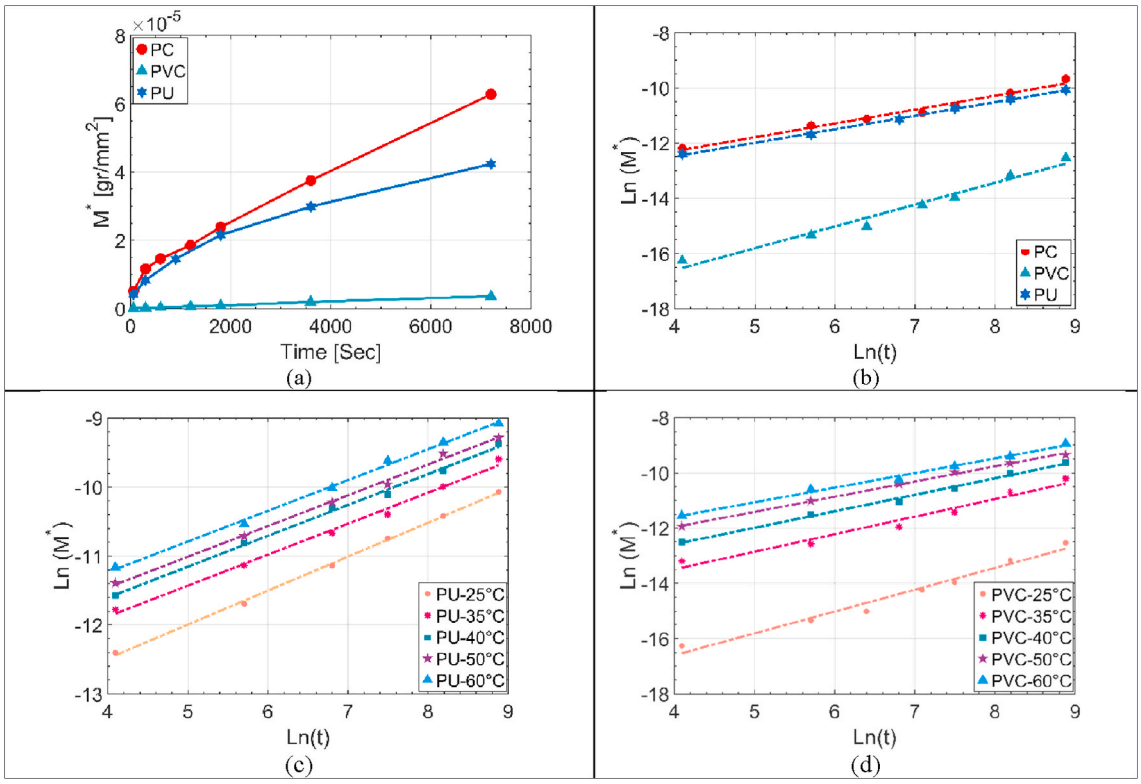

Fig. 11. (a) Resin uptake vs. time for TPs, (b) Ln(M*) vs. Ln(t) for different TPs at 25 °C, and for each TP of (c) PU, and (d) PVC at different temperatures.

Table 3
Empirical rate constant (k), and transport exponent (n) for each TP at different temperatures.

	PC		PU		PVC	
	n	k	n	k	n	k
25 °C	0.5001	6.09×10^{-7}	0.4921	5.27×10^{-7}	0.7901	2.61×10^{-9}
35 °C	–	–	0.4493	1.14×10^{-6}	0.6354	1.08×10^{-7}
40 °C	–	–	0.4479	1.15×10^{-6}	0.5972	3.13×10^{-7}
50 °C	–	–	0.4462	1.77×10^{-6}	0.5493	7.06×10^{-7}
60 °C	–	–	0.4461	2.21×10^{-6}	0.5305	1.09×10^{-6}

tool to predict the affinity between TPs with UPR were used to select TPs namely PEI, PVC, PU, and PC with different levels of affinities to UPR and to study the effect of affinity on the interphase thickness. It was realized that high affinity of PMMA leads to its dissolution into the UPR and while low affinity of PEI resulted in no proper interphase therefore they were eliminated from further investigations. The effect of processing temperature ranging from 4 °C to 60 °C was examined and it was observed that a change in the process temperature influenced the interphase thickness which was closely linked to the curing of the resin, diffusion kinetics and the physical state of TPs. The swelling of TPs in

Table 4
k_1, k_2, A_n and N_0 fit values in Eq. (5) and Eq. (6).

	K_1	K_2	A_n	N_0
PU	1.32×10^{-5}	4.64×10^{-8}	0.211	241
PVC	9.90×10^{-6}	9.90×10^{-6}	0.0185	1101

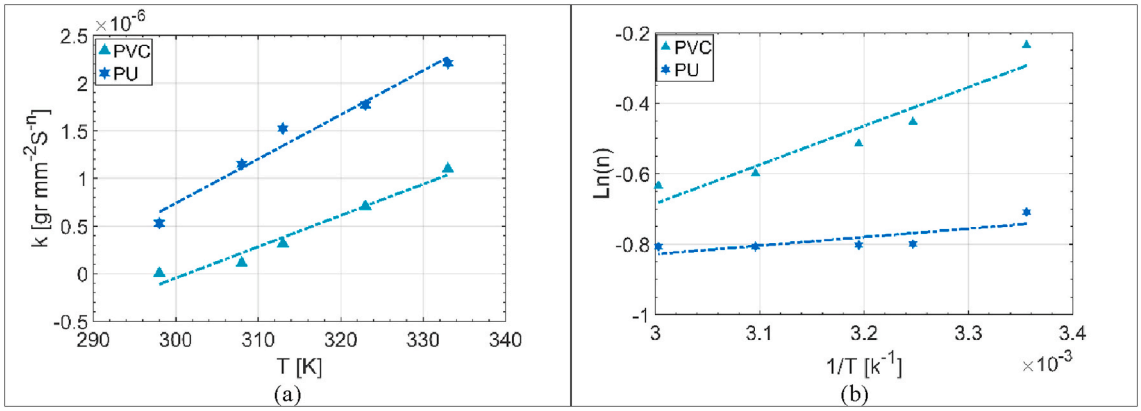

Fig. 12. (a) Empirical rate constant k, and (b) transport exponent n temperature dependency.

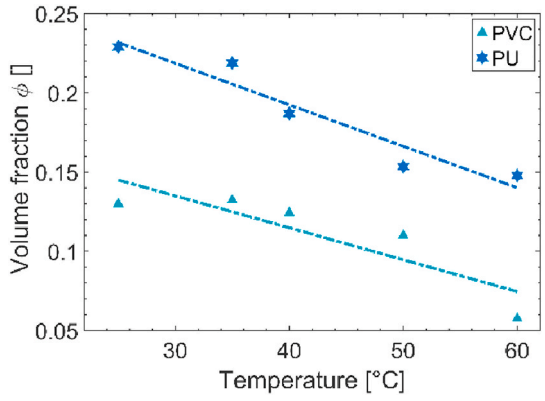

Fig. 13. Volume fraction of resin at the interphase (ϕ) vs processing temperatures obtained from Eq. (11).

contact with UPR was confirmed by confocal measurements and it was observed that the degree of swellings was correlated with HSPs affinity level. The kinetics of UPR diffusion were examined by resin uptake experiments which uncovered that the diffusion of UPR into PC and PU at 25 °C falls within the Fickian diffusion category while diffusion into PVC is an anomalous diffusion. The difference in the diffusion mechanisms for each TP was linked to the variations in the concentration gradient in the microscopic observations of interphases. A model to predict the UPR uptake considering different processing temperature was developed and the temperature dependency of parameters were extracted. Consequently, a model capable of predicting resin uptake for TPs at different temperatures was established. A coarse grain lattice model was employed to relate the resin uptake to the microscopic observation of interphase thickness and provided meaningful prediction on the microstructure of interphases through volume fraction of resin at the interphase. Furthermore, the authors are currently working on comprehensive microstructure analysis and micromechanical testing and their correlation to CGL model in various material combinations as an extension to this study.

Declaration of competing interest

The authors declare that they have no known competing financial interests or personal relationships that could have appeared to influence the work reported in this paper.

Acknowledgment

Authors gratefully acknowledge the research program Talent Scheme (Veni) with project number 15897, which is (partly) financed by the Netherlands Organization for Scientific Research (NWO) and TKI-Wind op Zee Topsector Energy subsidy from the Ministry of Economic Affairs, the Netherlands with the reference number TEWZ118008. Authors are also thankful to LM Wind Power for consultations during the project and supply polyester resin.

Appendix A. Supplementary data

Supplementary data to this article can be found online at https://doi.org/10.1016/j.polymer.2020.122991.

References

[1] C. Ageorges, L. Ye, Resistance welding of thermosetting composite/thermoplastic composite joints, Compos. Appl. Sci. Manuf. 32 (11) (2001) 1603–1612.
[2] J.S. Monfared Zanjani, B.S. Okan, Y.Z. Menceloglu, M. Yildiz, Nano-engineered design and manufacturing of high-performance epoxy matrix composites with carbon fiber/selectively integrated graphene as multi-scale reinforcements, RSC Adv. 6 (12) (2016) 9495–9506.
[3] A. Asundi, A.Y. Choi, Fiber metal laminates: an advanced material for future aircraft, J. Mater. Process. Technol. 63 (1–3) (1997) 384–394.
[4] M.R. Abdullah, Y. Prawoto, W.J. Cantwell, Interfacial fracture of the fibre-metal laminates based on fibre reinforced thermoplastics, Mater. Des. 66 (2015) 446–452.
[5] S. Arjula, A.P. Harsha, Study of erosion efficiency of polymers and polymer composites, Polym. Test. 25 (2) (2006) 188–196.
[6] E. Selver, P. Potluri, P. Hogg, C. Soutis, Impact damage tolerance of thermoset composites reinforced with hybrid commingled yarns, Compos. B Eng. 91 (2016) 522–538.
[7] S.D. Thoppul, J. Finegan, R.F. Gibson, Mechanics of mechanically fastened joints in polymer–matrix composite structures – a review, Compos. Sci. Technol. 69 (3) (2009) 301–329.
[8] T. Takeda, T. Yasuoka, H. Hoshi, S. Sugimoto, Y. Iwahori, Effectiveness of flame-based surface treatment for adhesive bonding of carbon fiber reinforced epoxy matrix composites, Compos. Appl. Sci. Manuf. 119 (2019) 30–37.
[9] D. Brassard, M. Dubé, J.R. Tavares, Resistance welding of thermoplastic composites with a nanocomposite heating element, Compos. B Eng. 165 (2019) 779–784.
[10] I. Baran, Warpage prediction in over-infusion process of glass/polyester composite laminates, in: 21st International Conference on Composite Materials, 2017, 2017.
[11] C. Leone, S. Genna, Effects of surface laser treatment on direct co-bonding strength of CFRP laminates, Compos. Struct. 194 (2018) 240–251.
[12] G. Rajagopalan, K.M. Immordino, J.W. Gillespie, S.H. McKnight, Diffusion and reaction of epoxy and amine in polysulfone studied using Fourier transform infrared spectroscopy: experimental results, Polymer 41 (7) (2000) 2591–2602.
[13] G. Rajagopalan, C. Narayanan, J.W. Gillespie, S.H. McKnight, Diffusion and reaction of epoxy and amine in polysulfone-transport modeling and experimental validation, Polymer 41 (24) (2000) 8543–8556.
[14] G. Rajagopalan, J.W. Gillespie Jr., S.H. McKnight, Diffusion of reacting epoxy and amine monomers in polysulfone: a diffusivity model, Polymer 41 (21) (2000) 7723–7733.
[15] P. Van Velthem, W. Ballout, D. Daoust, M. Sclavons, F. Cordenier, E. Henry, D. Dumont, V. Destoop, T. Pardoen, C. Bailly, Influence of thermoplastic diffusion on morphology gradient and on delamination toughness of RTM-manufactured composites, Compos. Appl. Sci. Manuf. 72 (2015) 175–183.
[16] Q. Voleppe, T. Pardoen, C. Bailly, Interdiffusion and phase separation upon curing in thermoset-thermoplastic interphases unravelled by the characterization of partially cured systems, Polymer 106 (2016) 120–127.
[17] C. Sonnenfeld, H. Mendil-Jakani, R. Agogué, P. Nunez, P. Beauchêne, Thermoplastic/thermoset multilayer composites: a way to improve the impact damage tolerance of thermosetting resin matrix composites, Compos. Struct. 171 (2017) 298–305.
[18] H. Shi, J. Sinke, R. Benedictus, Surface modification of PEEK by UV irradiation for direct co-curing with carbon fibre reinforced epoxy prepregs, Int. J. Adhesion Adhes. 73 (2017) 51–57.
[19] F. Pierce, D. Perahia, G.S. Grest, Interdiffusion of short chain oligomers into an entangled polymer film, Macromolecules 42 (20) (2009) 7969–7973.
[20] S. Deng, L. Djukic, R. Paton, L. Ye, Thermoplastic–epoxy interactions and their potential applications in joining composite structures – a review, Compos. Appl. Sci. Manuf. 68 (2015) 121–132.
[21] I.F. Villegas, R. van Moorleghem, Ultrasonic welding of carbon/epoxy and carbon/PEEK composites through a PEI thermoplastic coupling layer, Compos. Appl. Sci. Manuf. 109 (2018) 75–83.
[22] C.M. Hansen, Hansen Solubility Parameters: a User's Handbook, CRC press, 2002.
[23] J. Seyyed Monfared Zanjani, B. Saner Okan, I. Letofsky-Papst, M. Yildiz, Y. Z. Menceloglu, Rational design and direct fabrication of multi-walled hollow electrospun fibers with controllable structure and surface properties, Eur. Polym. J. 62 (2015) 66–76.
[24] Z. Kurban, A. Lovell, S.M. Bennington, D.W.K. Jenkins, K.R. Ryan, M.O. Jones, N. T. Skipper, W.I.F. David, A solution selection model for coaxial electrospinning and its application to nanostructured hydrogen storage materials, J. Phys. Chem. C 114 (49) (2010) 21201–21213.
[25] N. Deslandes, V. Bellenger, F. Jaffiol, J. Verdu, Solubility parameter of a polyester composite material, J. Appl. Polym. Sci. 69 (13) (1998) 2663–2671.
[26] R. Dunnigan, J. Clemens, M.N. Cavalli, N. Kaabouch, S. Gupta, Beneficial usage of recycled polymer particulates for designing novel 3D printed composites, Addit. Manuf. 3 (1) (2018) 33–38.
[27] C. Hsu, L.J. Lee, Free-radical crosslinking copolymerization of styrene/unsaturated polyester resins: 3. Kinetics-gelation mechanism, Polymer 34 (21) (1993) 4516–4523.
[28] P.E. Shaw, P.L. Burn, Real-time fluorescence quenching-based detection of nitro-containing explosive vapours: what are the key processes? Phys. Chem. Chem. Phys. 19 (44) (2017) 29714–29730.
[29] L.H. Sperling, Interpenetrating Polymer Networks: an Overview, Interpenetrating Polymer Networks, American Chemical Society, 1994, pp. 3–38.
[30] L.-J. Vandi, M. Hou, M. Veidt, R. Truss, M. Heitzmann, R. Paton, Interface diffusion and morphology of aerospace grade epoxy co-cured with thermoplastic polymers, in: 28th International Congress of the Aeronautical Sciences (ICAS), 2012, pp. 23–28. Brisbane, Australia, Sept.
[31] C.Y. Hui, K.C. Wu, R.C. Lasky, E.J. Kramer, Case-II diffusion in polymers. I. Transient swelling, J. Appl. Phys. 61 (11) (1987) 5129–5136.